Spring 5-2-2011

Simulation of Particle-Gas Flow in a Cyclone Using URANS

Aku Karvinen
Tampere University of Technology

Hannu Ahlstedt
Tampere University of Technology

Marko Palonen
Metso Power Oy

SIMULATION OF PARTICLE-GAS FLOW IN CYCLONE USING URANS

Aku Karvinen and Hannu Ahlstedt
Tampere University of Technology
PO Box 589, FI-33101 Tampere, Finland

Marko Palonen
Metso Power Oy
PO Box 109, FI-33101 Tampere, Finland

ABSTRACT

Particle-gas flow in a cyclone separator used in a circulating fluidized-bed boiler is simulated using computational fluid dynamics software Fluent 6.2.36 and an Unsteady Reynolds-Averaged Navier-Stokes (URANS) method. A Lagrangian method is used for particle simulation and a one-way coupling between particles and gas is assumed. The effect of the turbulence model is studied using several turbulence models. Only the Reynolds stress model gives a physically reasonable flow field without adjusting parameters unknown beforehand.

INTRODUCTION

Cyclone separators (Fig. 1) occur in many industries, e.g. in oil and gas industry, power generation, incineration plants, cement plants, coking plants and the food industry. Compared to the other methods for particle removal from gases the main advantages of cyclone separators are: low capital investment and maintenance costs, applicability under extreme processing conditions, no moving parts, and robustness.

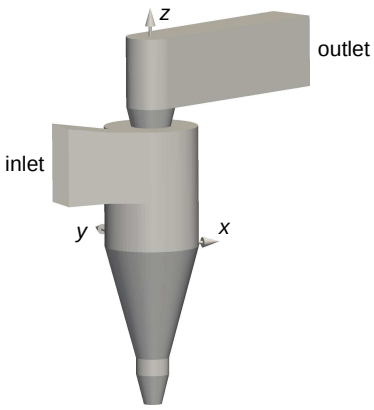

Figure 1: Cyclone separator. Domain and coordinate system used in this study.

According to (1), the first studies of the cyclone flow were undertaken in 1930-1950 (2) and (3). The first CFD (computational fluid dynamics) simulations were undertaken in the 80's (4). In the 21st century, CFD simulations have been made for example by Derksen (5) and by Wang (6). A more extensive review can be found in (7) and (1).

CASE STUDIED

The schematic of the case studied and the coordinate system used is given in Fig. 1. The flow gas is hot air. The cyclone body Reynolds number based on an average inlet velocity and the cyclone diameter (7) is Re = 634,000.

METHODS AND MODELS

The Reynolds-averaged Navier-Stokes equations (RANS) for incompressible flow are

$$\frac{\partial u_i}{\partial x_i} = 0, \tag{1}$$

$$\frac{\partial u_i}{\partial t} + u_j \frac{\partial u_i}{\partial x_j} = -\frac{1}{\rho}\frac{\partial p}{\partial x_i} + \nu \frac{\partial^2 u_i}{\partial x_j \partial x_j} + \frac{\partial}{\partial x_j}\left(-\overline{u_i' u_j'}\right), \tag{2}$$

where the overbar denotes time averaging, and the prime denotes the fluctuating component. In the k-ε models and the k-ω models, the Boussinesq hypothesis is used in which the Reynolds stresses, $-\overline{u_i' u_j'}$, are calculated from

$$-\overline{u_i' u_j'} = 2\nu_t S_{ij} - \frac{2}{3} k \delta_{ij}, \quad S_{ij} = \frac{1}{2}\left(\frac{\partial u_i}{\partial x_j} + \frac{\partial u_j}{\partial x_i}\right). \tag{3}$$

In **the standard k-ε model** (8), the turbulence kinetic energy and its dissipation rate are obtained from the modeled transport equations, which are as follows:

$$\frac{\partial k}{\partial t} + u_j \frac{\partial k}{\partial x_j} = \frac{\partial}{\partial x_j}\left[\left(\nu + \frac{\nu_t}{\sigma_k}\right)\frac{\partial k}{\partial x_j}\right] + \nu_t S^2 - \varepsilon, \tag{4}$$

$$\frac{\partial \varepsilon}{\partial t} + u_j \frac{\partial \varepsilon}{\partial x_j} = \frac{\partial}{\partial x_j}\left[\left(\nu + \frac{\nu_t}{\sigma_\varepsilon}\right)\frac{\partial \varepsilon}{\partial x_j}\right] + C_{1\varepsilon}\frac{\varepsilon}{k}\nu_t S^2 - C_{2\varepsilon}\frac{\varepsilon^2}{k}, \tag{5}$$

where $S \equiv \sqrt{2 S_{ij} S_{ij}}$. The turbulent viscosity is computed from $\nu_t = C_\mu k^2/\varepsilon$. Model constants used have the following values: C_μ = 0.09, $C_{1\varepsilon}$ = 1.44, $C_{2\varepsilon}$ = 1.92, σ_k = 1.0, and σ_ε = 1.3.

The transport equations for k and ε in **the RNG k-ε model** (9) are

$$\frac{\partial k}{\partial t} + u_j \frac{\partial k}{\partial x_j} = \frac{\partial}{\partial x_j}\left(\alpha_k \nu_t \frac{\partial k}{\partial x_j}\right) + \nu_t S^2 - \varepsilon, \tag{6}$$

$$\frac{\partial \varepsilon}{\partial t} + u_j \frac{\partial \varepsilon}{\partial x_j} = \frac{\partial}{\partial x_j}\left(\alpha_\varepsilon \nu_t \frac{\partial \varepsilon}{\partial x_j}\right) + C_{1\varepsilon}\frac{\varepsilon}{k}\nu_t S^2 - C_{2\varepsilon}\frac{\varepsilon^2}{k} - \frac{C_\mu \eta^3 (1 - \eta/\eta_0)}{1 + \beta\eta^3}\frac{\varepsilon^2}{k}, \tag{7}$$

where $\eta \equiv Sk/\varepsilon$, η_0 = 4.38, β = 0.012, and ν_t is obtained in a similar way as in the standard k-ε model. The model constants are: C_μ = 0.0845, $C_{1\varepsilon}$ = 1.42, and $C_{2\varepsilon}$ = 1.68.

The RNG k-ε model in Fluent provides an option to account for the effects of the swirl in the mean flow by modifying the turbulent viscosity appropriately:

$$\nu_{t,\text{modified}} = \nu_t f\left(\alpha_s, \Omega, \frac{k}{\varepsilon}\right), \tag{8}$$

where Ω is a swirl number evaluated within Fluent and α_s is a swirl constant that assumes different values depending on whether the flow is swirl-dominated or mildly swirling. The exact function for describing this dependency is not revealed in (10).

The transport equations for k and ε in **the realizable k-ε model** (11), (10) are

$$\frac{\partial k}{\partial t} + u_j \frac{\partial k}{\partial x_j} = \frac{\partial}{\partial x_j}\left[\left(\nu + \frac{\nu_t}{\sigma_k}\right)\frac{\partial k}{\partial x_j}\right] + \nu_t S^2 - \varepsilon, \tag{9}$$

$$\frac{\partial \varepsilon}{\partial t} + u_j \frac{\partial \varepsilon}{\partial x_j} = \frac{\partial}{\partial x_j}\left[\left(\nu + \frac{\nu_t}{\sigma_\varepsilon}\right)\frac{\partial \varepsilon}{\partial x_j}\right] + C_{1\varepsilon} S\varepsilon - C_{2\varepsilon}\frac{\varepsilon^2}{k + \sqrt{\nu\varepsilon}}, \tag{10}$$

where $C_{1\varepsilon}$ is now a variable. The turbulent viscosity is obtained in a similar way as in the standard k-ε model, but C_μ is no longer constant. The model constants are: $C_{2\varepsilon}$ = 1.9, σ_k = 1.0, and σ_ε = 1.2.

In **the standard k-ω model** (12), the turbulence kinetic energy, k, and the specific dissipation rate, ω, are obtained from the following transport equations:

$$\frac{\partial k}{\partial t} + u_j \frac{\partial k}{\partial x_j} = \frac{\partial}{\partial x_j}\left[\left(\nu + \frac{\nu_t}{\sigma_k}\right)\frac{\partial k}{\partial x_j}\right] + \nu_t S^2 - \beta^*_\infty f_{\beta^*} k\omega, \tag{11}$$

$$\frac{\partial \varepsilon}{\partial t} + u_j \frac{\partial \omega}{\partial x_j} = \frac{\partial}{\partial x_j}\left[\left(\nu + \frac{\nu_t}{\sigma_\omega}\right)\frac{\partial \omega}{\partial x_j}\right] + \frac{\omega}{k}\nu_t S^2 - \beta_i f_\beta \omega^2, \tag{12}$$

and the turbulent viscosity is obtained from $\nu_t = k/\omega$. The model constants are: β_i = 0.072, β^*_∞ = 0.09, σ_k = 2.0, and σ_ω = 2.0.

The SST k-ω model (13) has a form similar to that of the standard k-ω model. The transport equations are given as follows

$$\frac{\partial k}{\partial t} + u_j \frac{\partial k}{\partial x_j} = \frac{\partial}{\partial x_j}\left[\left(\nu + \frac{\nu_t}{\sigma_k}\right)\frac{\partial k}{\partial x_j}\right] + \min(\nu_t S^2, 10\rho\beta^*_\infty k\omega) - \beta^*_\infty k\omega, \tag{13}$$

$$\frac{\partial \varepsilon}{\partial t} + u_j \frac{\partial \omega}{\partial x_j} = \frac{\partial}{\partial x_j}\left[\left(\nu + \frac{\nu_t}{\sigma_\omega}\right)\frac{\partial \omega}{\partial x_j}\right] + S^2 - \beta_i \omega^2 + D_\omega, \tag{14}$$

where $\beta_i = F_1\beta_{i,1} + (1 - F_1)\beta_{i,2}$ and σ_k and σ_ω are calculated in a similar way. The turbulent viscosity $\nu_t = (k/\omega)/\max[1, SF_2/(a_1\omega)]$. The model constants are: a_1 = 0.31, β^*_∞ = 0.09, $\beta_{i,1}$ = 0.075, $\beta_{i,2}$ = 0.0828, $\sigma_{k,1}$ = 1.176, $\sigma_{\omega,1}$ = 2.0, $\sigma_{k,2}$ = 1.0, and $\sigma_{\omega,2}$ = 1.168.

In **the Reynolds stress model (RSM)**, there are the exact transport equations for the transport of Reynolds stresses, $-\overline{u_i' u_j'}$ (14):

$$\frac{\partial \overline{u_i' u_j'}}{\partial t} + \frac{\partial}{\partial x_k}\left(u_k \overline{u_i' u_j'}\right) = \underbrace{-\frac{\partial}{\partial x_k}\left[\overline{u_i' u_j' u_k'} + \overline{\frac{p'}{\rho}\left(\delta_{kj} u_i' + \delta_{ik} u_j'\right)}\right]}_{D^t_{ij}} + \frac{\partial}{\partial x_k}\left[\nu \frac{\partial}{\partial x_k}\left(\overline{u_i' u_j'}\right)\right]$$

$$- \left(\overline{u_i' u_k'}\frac{\partial u_j}{\partial x_k} + \overline{u_j' u_k'}\frac{\partial u_i}{\partial x_k}\right) + \underbrace{\overline{\frac{p'}{\rho}\left(\frac{\partial u_i'}{\partial x_j} + \frac{\partial u_j'}{\partial x_i}\right)}}_{\phi_{ij}} - \underbrace{2\nu\overline{\frac{\partial u_i'}{\partial x_k}\frac{\partial u_j'}{\partial x_k}}}_{\varepsilon_{ij}}, \tag{15}$$

where D_{ij}^{t}, ϕ_{ij}, and ε_{ij} are modeled, see (10) for more details. The model constants are: C_1 = 1.8, C_2 = 0.60, $C_{1\varepsilon}$ = 1.44, $C_{2\varepsilon}$ = 1.92, C_μ = 0.9, σ_k = 1.0, and σ_ε = 1.3.

Calculation Procedure and Computational Grid

All the calculations are performed using commercial software Fluent 6.3.26 (10). All terms in all equations are discretized in space using second-order central differencing, apart from the convection term, which is discretized using a second-order upwind scheme. Pressure-velocity coupling is achieved using the PISO algorithm.

Time integration is done using a first order implicit method and adaptive time stepping where the first time step is very small ($\Delta t_0 = 10^{-6}$ s) and next time steps are chosen as follows: If the solution has not converged after seven iterations, then $\Delta t_{\text{new}} = 0.9\Delta t_{\text{old}}$, otherwise, $\Delta t_{\text{new}} = 1.1\Delta t_{\text{old}}$.

The simulation is initiated using a steady state solver. After several thousand iterations, the simulation is continued by running an unsteady solver and run until the flow becomes statistically steady (30 s). After that, simulation is continued until statistically stable data is gathered (30 s $\rightarrow$ 60 s).

The computational grid consists exclusively of hexahedral cells (Fig. 2). Four different grid resolutions have been used such that the total number of control volumes used is 72,978, 260,808, 785,819 or 1,802,564. All grids are constructed so that the grid is finer for the wall-adjacent cells of all no-slip walls of the cyclone.

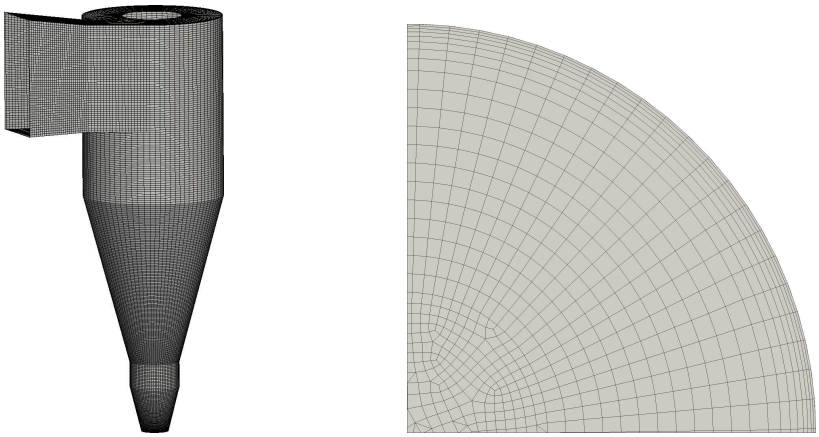

(a) In inlet and cyclone walls.

(b) In middle of cyclone barrel in positive quadrant.

Figure 2: Grid 785,819.

GRID INDEPENDENCY TEST

The grid independency test shows that velocity profiles of the RSM in the middle of the cyclone barrel do not change significantly when the grid is made finer than 785,819

cells (Fig. 3). A grid of 785,819 cells is therefore used exclusively in the turbulence model comparison. A dimensionless wall unit y^+ in a cyclone barrel is in an acceptable range (within the log-law layer) when a 785,819 grid is used (Fig. 3(d)).

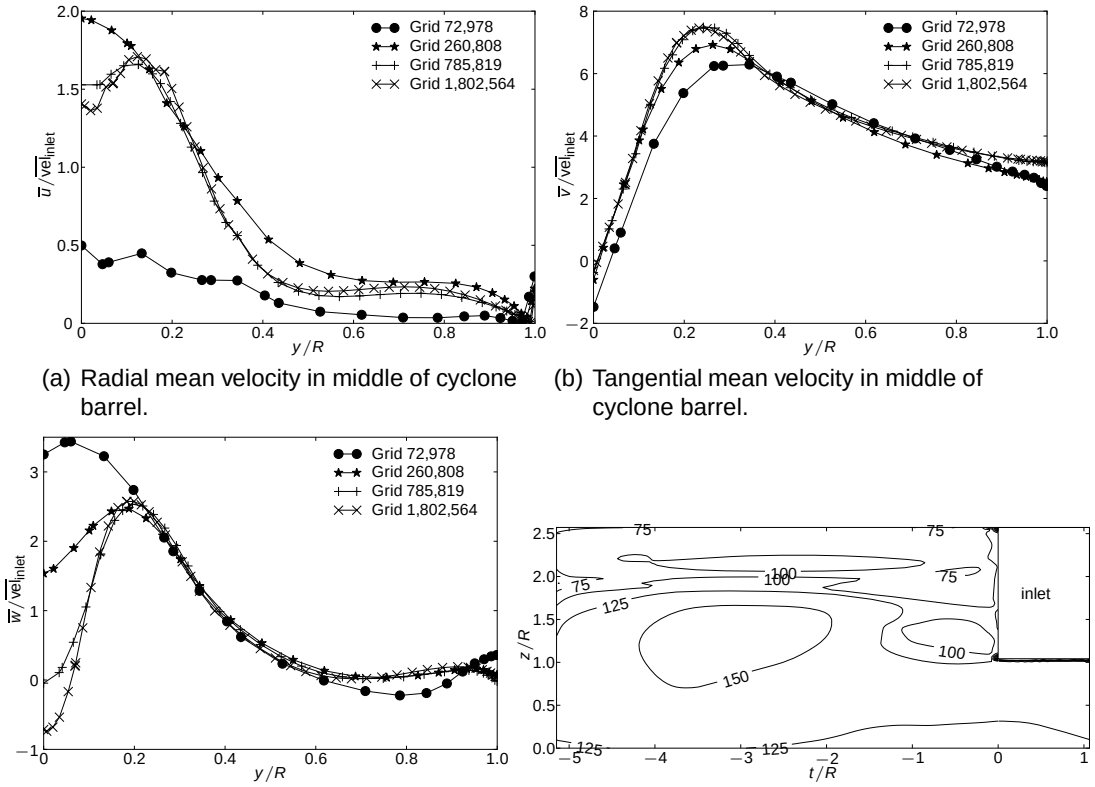

(a) Radial mean velocity in middle of cyclone barrel.

(b) Tangential mean velocity in middle of cyclone barrel.

(c) Axial mean velocity in middle of cyclone barrel.

(d) Dimensionless wall unit y^+ in cyclone barrel looked inside out. Grid 785,819.

Figure 3: Grid independency test.

TURBULENCE MODEL COMPARISON

Several papers, e.g. (7) and (1), show that there is rigid body rotation in the core of the cyclone and almost friction free flow in the outer part of the cyclone. Tangential velocity profiles complying with these assumptions are shown in Fig. 4(b) by the dashed lines (constants are adjusted according to the results of the RSM).

Because of the highly anisotropic turbulence caused by the high curvature of the streamlines and the high swirl intensity, two equation models cannot predict the flow field correctly – they predict almost rigid body rotation in the whole flow field. Only the RSM gives a physically reasonable flow field.

The RNG k-ε model with swirl modification implemented in Fluent gives usable results, but the modification contains an adjustable parameter which was unknown before the simulations. The default value of the parameter is α_s = 0.07, which turns out to be too small, as can be seen in Fig. 4(b). This makes the modification difficult to use.

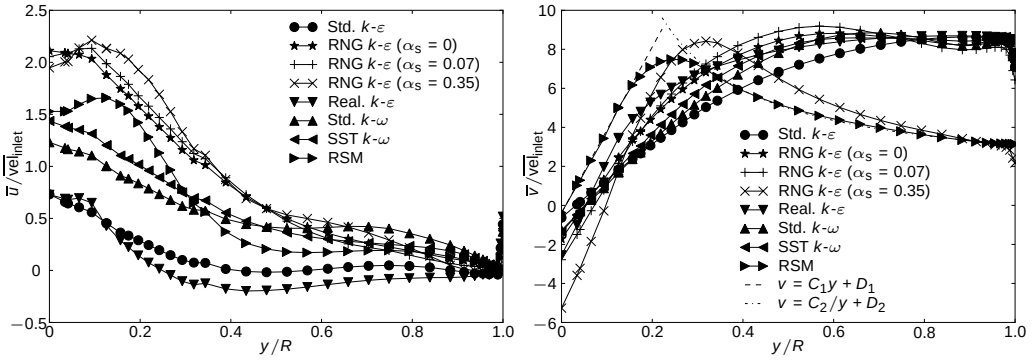

(a) Radial mean velocity.

(b) Tangential mean velocity.

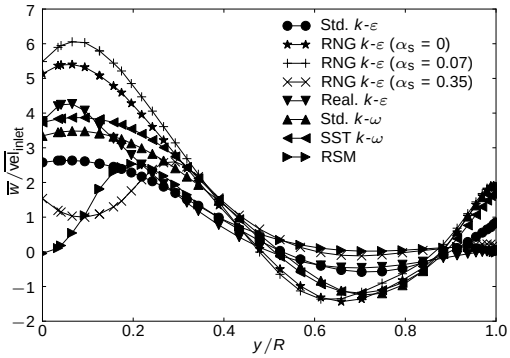

(c) Axial mean velocity.

Figure 4: Turbulence model comparison.

PARTICLE TRAJECTORY SIMULATION

Because the only turbulence model that gives a reasonable flow field without any adjustable parameter is the RSM, particle trajectory simulation is only done using that model. Particles of different size are released from the bed and the particle trajectories are calculated assuming one-way coupling (particles do not affect the flow field). The mean flow field is used and no turbulence effects on particles are taken into account. The collision chart in the cyclone barrel is shown in the Fig. 5(a). The collision area of the largest particle corresponds well with the largest measured erosion (Fig. 5(b)).

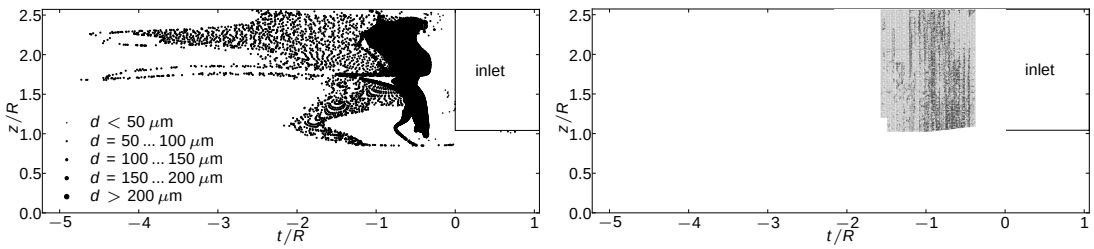

(a) Simulated collision chart. RSM.

(b) Measured erosion in target zone. Darkest gray denotes largest erosion.

Figure 5: Simulated collision chart and measured erosion.

CONCLUSIONS

An extensive grid independency test is achieved using the Reynolds stress model (RSM). The number of the cells in grids varies between 72,978 and 1,802,564. The grid independency test shows that a grid consisting of about 800,000 cells gives acceptable results.

An effect of the turbulence model is studied using six different turbulence models. Because of the highly anisotropic turbulence caused by the high curvature of the streamlines and the high swirl intensity, two equation models cannot predict the flow field correctly. Only the RSM gives a physically reasonable flow field. Also the RNG k-ε model with a swirl modification implemented in Fluent gives usable results, but the modification contains an adjustable parameter which was unknown before the simulations. When the RSM is used, the collision area of the largest particle corresponds well with the largest measured erosion.

ACKNOWLEDGMENT

The authors gratefully acknowledge the support from Metso Power Oy and from The Finnish Graduate School in Computational Fluid Dynamics.

NOTATION

C_μ, C_1, C_2, $C_{1\varepsilon}$, $C_{2\varepsilon}$	model constant in turbulence models
D_{ij}^{t}	turbulent diffusive transport tensor in RSM
D_ω	cross-diffusion term in RNG k-ε model
F_1, F_2	blending functions in SST k-ω model
P_{ij}	stress production tensor in RSM
R	radius of cyclone barrel
Re	cyclone body Reynolds number
S	mean rate-of-strain tensor
d	particle diameter
f_{β^*}, f_β	auxiliary functions in standard k-ω model
k	turbulent kinetic energy
p	mean pressure
t	time, tangential coordinate
Δt_0, Δt_{old}, Δt_{new}	first, old and new time steps
$\overline{u}$, $\overline{v}$, $\overline{w}$	mean velocity components
$\overline{\mathrm{vel}}_{\mathrm{inlet}}$	average mean velocity in beginning of inlet
y^+	dimensionless wall unit
Ω	mean rate-of-rotation, characteristic swirl number
α_k, α_ε	inverse effective Prandtl numbers
α_{s}	swirl constant in RNG k-ε model
β_i, β_∞^*, $\beta_{i,1}$, $\beta_{i,2}$	model constants in turbulence models
δ	Kronecker delta
ε	dissipation rate of turbulent kinetic energy
ε_{ij}	dissipation tensor in RSM

ν, ν_t	molecular and turbulent kinematic viscosity
$\nu_{t,modified}$	modified turbulent kinematic viscosity
ϕ_{ij}	pressure-strain tensor in RSM
ρ	density
σ_k, σ_ε, σ_ω, $\sigma_{k,1}$, $\sigma_{k,2}$, $\sigma_{\omega,1}$, $\sigma_{\omega,2}$	model constants in turbulence models
σ_k, σ_ω	auxiliary functions in SST k-ω model

REFERENCES

1. C. Cortés and A. Gil. Modeling the gas and particle flow inside cyclone separators. *Progress in Energy and Combustion Science*, 33(5):409–452, 2007.
2. R. M. C. K. Alexander. Fundamentals of cyclone design and operation. *Proceedings of the Australasian Institute of Mining and Metallurgy*, 152:208–228, 1949.
3. A. J. Linden. Investigation into cyclone dust collectors. *Proceedings of the Institution of Mechanical Engineers*, 160:233–251, 1949.
4. F. Boysan, W. H. Ayers, and J. Swithenbank. A fundamental mathematical modelling approach to cyclone design. *Transactions of the American Institute of Chemical Engineers*, 60:222–230, 1982.
5. J. J. Derksen, S. Sundaresan, and H. E. A. van den Akker. Simulation of mass-loading effects in gas-solid cyclone separators. *Powder Technology*, 163:59–68, 2006.
6. B. Wang, D. L. Xu, K. W. Chu, and A. B. Yu. Numerical study of gas-solid flow in a cyclone separator. *Applied Mathematical Modelling*, 30:1326–1342, 2006.
7. A. C. Hoffmann and L. E. Stein. *Gas Cyclones and Swirl Tubes: Principles, Design and Operation*. Springer, Berlin, 2002.
8. B. E. Launder and D. B. Spalding. *Lectures in Mathematical Models of Turbulence*. Academic Press, London, 1972.
9. V. Yakhot and S. A. Orszag. Renormalization group analysis of turbulence. *Physical Review Letters*, 57:1722–1724, 1986.
10. Fluent Inc. FLUENT 6.3 User's Guide. Lebanon, 2006.
11. T.-H. Shih, W. W. Liou, A Shabbir, Z. Yang, and J. Zhu. A new k-ε eddy viscosity model for high Reynolds number turbulent flows. *Computers and Fluids*, 24:227–238, 1995.
12. D. C. Wilcox. *Turbulence Modeling for CFD*. DCW Industries, Inc., La Canada, California, second edition, 1998.
13. F. R. Menter. Two-equation eddy-viscosity turbulence models for engineering applications. *AIAA Journal*, 32:1598–1605, 1994.
14. M. M. Gibson and B. E. Launder. Ground effects on pressure fluctuations in the atmospheric boundary layer. *Journal of Fluid Mechanics*, 86:491–511, 1978.